*Invited Paper*

# Investigation of the tapered waveguide structures for terahertz quantum cascade lasers

T. H. Xu, and J. C. Cao *
Key Laboratory of Terahertz Solid-State Technology, Shanghai Institute of Microsystem and Information Technology, Chinese Academy of Sciences, Shanghai, 200050, China
* Email: jccao@mail.sim.ac.cn

(Received August 18, 2015)

**Abstract**: The authors present a quasi-three-dimensional numerical simulation model based on the beam propagation method, which is suitable to simulate and design terahertz quantum cascade lasers with non-uniform axial waveguide structure. Using this simulation model, various kinds of tapered terahertz quantum cascade lasers were studied. According to our analysis, the normal tapered waveguide structure, although is simple, is a good choice to achieve good output beam quality and high output power simultaneously.

**Keywords**: Beam propagation method, Terahertz quantum cascade laser, Beam quality, Tapered, Numerical simulation

**doi:** 10.11906/TST.119-128.2015.09.12

## 1. Introduction

The first mid-infrared quantum cascade laser (QCL) has been realized in 1994 [1]. Since then, researches kept on making progress in the performances of this kind of devices in the terms of the lasing frequency range, the working temperature and the output power. Later, in 2002, the first terahertz (THz) QCL in the world has been realized [2], which broke through the vacancy of the THz solid-state source. In last few years, especially, great interests have been attracted into the researches of the THz related technologies [3, 4], due to the potential applications of them in the fields of material analysis, security imaging and wireless communication [5]. So far, THz QCLs in continuous wave (CW) mode have achieved output power of 138 *mW* [6] and working temperature of 117 *K* [7]. While, for THz QCLs in pulsed mode, the highest output power is 1 *W* [8] and the highest operating temperature is 186 *K* [9]. In addition, there are also some THz QCLs with specific functions, such as the single mode THz QCL based on distributed feedback technology [10] and THz comb [11].

Traditional THz QCL always has the straight strip waveguide structure. In order to prevent high order lateral modes, the straight THz QCL always has limited ridge width from tens of

micron to hundreds of micron, which is within the sub-wavelength range. A general problem for this kind of device is that the radiation field from it always has large far field divergence angle and poor beam quality. It has already been demonstrated experimentally that previous mentioned problem could be solved in a certain extent by using the tapered waveguide structure [12]. However, the optimum taper angle is difficult to be decided in advance. In order to simplify the design process of the THz QCL with non-uniform axial waveguide structure, we have established a numerical simulation model based on the finite difference beam propagation method (FD-BPM). Indeed, simulation researches about THz QCL are rare in the literatures and mainly concentrated in the calculation of the two-dimensional lateral modes using the finite element method [13]. In this paper, a quasi-three-dimensional numerical model will be introduced, which is suitable to analyze the beam propagation process in the THz QCL with non-uniform axial waveguide structure. Especially, by introducing the rate equation method, which describes the carrier dynamics in the active region, the current induced changes in the gain and the refractive index are considered, making this numerical model suitable for the active devices also. Utilizing this numerical model, a few kinds of tapered THz QCL have been studied to search for the optimum waveguide structure which could achieve good beam quality and high output power simultaneously. The investigation results show that the traditional tapered structure, although it is simple, obtains the best performances.

## 2. The numerical simulation model

In this paper, we focus on the tapered THz QCLs lasing at $\lambda_0 = 103\ \mu m$, which have bound-to-continuum (BTC) active region and semi-insulating surface-plasma (SISP) waveguide structure (for other details about the device material please refer to [12]).

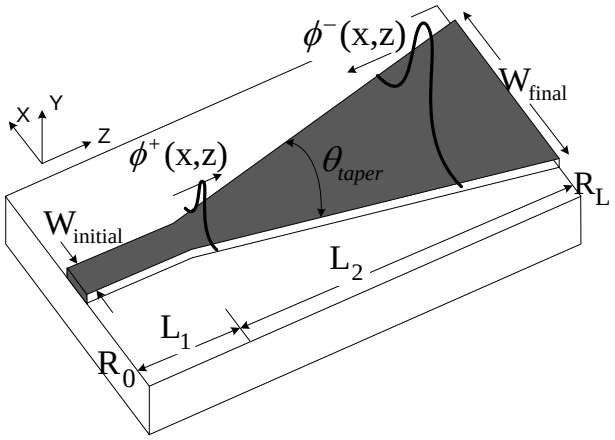


Fig. 1 3D schematic of the tapered THz QCL and the coordinates used in the numerical model.

The whole numerical model can be divided into three parts. The most important part is a

two-dimensional BPM equation, describing the electrical field evolution when it propagates inside the waveguide. While the second and the third parts are used to calculate the current injection independent/dependent parameters respectively, and these parameters are used in the BPM equation to describe the material properties of this device and to determine the optical field evolution. These three parts will be described one by one in the following parts of this paper.

The two-dimensional wave equation for the slowly varying components $\phi(x,z)$ of the electrical field inside the waveguide ( $E(x,z)=\phi(x,z)\exp(-jkn_0z)$ ) is a well known BPM second-order differential equation [14]:

$$\frac{\partial\phi(x,z)}{\partial z}=-j\frac{1}{2k_0n_0}\frac{\partial^2\phi}{\partial x^2}-j\frac{k_0}{2n_0}\left[n_{eff}(x,z)-n_0\right]^2\phi(x,z)-\frac{1}{2}\alpha_i(x,z)\phi(x,z)$$
$$+\frac{1}{2}g_m(x,z,J,S)\phi(x,z)-jk_0\Delta n(x,z,J,S)\phi(x,z) \quad (1)$$

where $k_0$ is the propagation constant, $n_0$ is the reference refractive index outside the active waveguide, $n_{eff}(x,z)$ and $\alpha_i(x,z)$ are, respectively, the distribution profile of the effective refractive index and the intrinsic waveguide in the x-z plane (see figure 1), $g_m(x,z,J,S)$ and $\Delta n(x,z,J,S)$ are, respectively, the distribution profile of the modal gain and the refractive index variation induced by interaction between the carriers and the photons. Therefore, $g_m$ and $\Delta n$ are dependent on the local current density *J* and the photon density *S*. The photon density *S* is proportional to the square of $\phi(x,z)$.

The traditional BPM model and the commercial BPM software are suitable for passive waveguide simulations. While in our numerical model, by adding $g_m$ and $\Delta n$ into the traditional BPM wave equation, the current injection induced variations in the modal gain and the refractive index are considered, so the dynamic changes of the optical field in the active devices could be simulated properly by this numerical model.

As we mentioned above, $n_{eff}$ and $\alpha_i$ are independent of the carrier variations, so they have fixed values during the simulation processes. However, they have different values in the regions inside/outside the active waveguide respective. By referring to the published literatures, the intrinsic loss inside the waveguide $\alpha_{i1}$ is set to 15 $cm^{-1}$[15], and for the outside region $\alpha_{i2}$ is set to 435 $cm^{-1}$[16].

In order to calculate the effective refractive index for the THz QCL, the following method is utilized: firstly, we calculate the complex refractive index $n$ for each epitaxial layer in the y direction using the Drude-Lorentz model (related parameters please refer to [14, 17]); then, we

supply the complex refractive indexes and the cross-section waveguide structure to a commercial software (COMSOL Multiphysics), which solves the Helmholtz equation based on the finite element method and gives the lateral mode profile and the effective refractive index of the simulated waveguide structure. Finally, we obtain that the effective refractive index inside the waveguide region ($n_{eff1}$) is 3.53, while for the outside region it ($n_{eff2}$) is 3.42.

For an active device, such as the THz QCL, the current injection induced modal gain changes due to the interaction between the carriers and the photons. The carrier dynamics within the active region could be appropriately described by a rate equation set with three energy levels. By solving the steady state solution of the rate equation set under different *J* and *S*, we can obtain the corresponding modal gain values $g_m(J,S)$ (for details please refer to [18]). Example results are shown in figure 2. We can see that when optical field is low, the modal gain has constant value and increases with the injection current density. However, when the photon density is quite high, the modal gain decreases rapidly and even goes to zero finally. This effect is one of the key reasons that leads to complex variations in the electric field when it propagates in an active device.

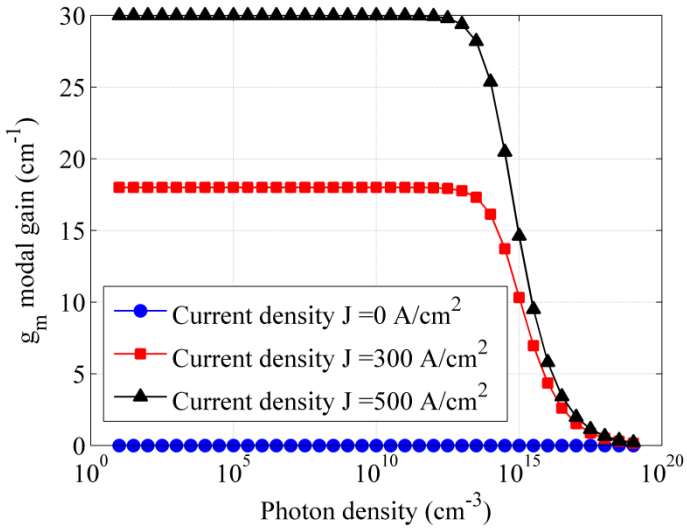


Fig. 2 The modal gain under different injection current densities and photon densities. We used blue circles, red squares and black upward-pointing triangles as markers when injection current density equals 0 *A/cm*$^2$, 300 *A/cm*$^2$ and 500 *A/cm*$^2$ respectively.

Based on the modal gain values, the related refractive index variation $\Delta n(J,S)$ induced by current injection is calculated using equation 2 [19].

$$\Delta n(J,S) = -\frac{\alpha_{LEF}}{2k_0} g_m(J,S) \tag{2}$$

where $\alpha_{LEF}$ is the linewidth enhancement factor (LEF), and $\alpha_{LEF}$ = 2.5 during the simulation.

Now all the parameters inside the BPM equation are obtained, then this theoretical model is built by MATLAB and solved numerically. The numerical simulation approach is described in details in [18].

## 3. Investigation of the tapered THz QCLs

Straight strip is the most popular used waveguide structure for THz QCLs, and large ridge width is always used to increase the output power for this kind of device. However, this method will lead to multiple lateral modes if the ridge width is too large. One method to get balance between high output power and good output beam quality is to utilize the tapered waveguide structure [12]. In order to investigate the influence of the tapered waveguide structure on the device performances, previous introduced BPM model is used to simulate four kinds of tapered THz QCL.

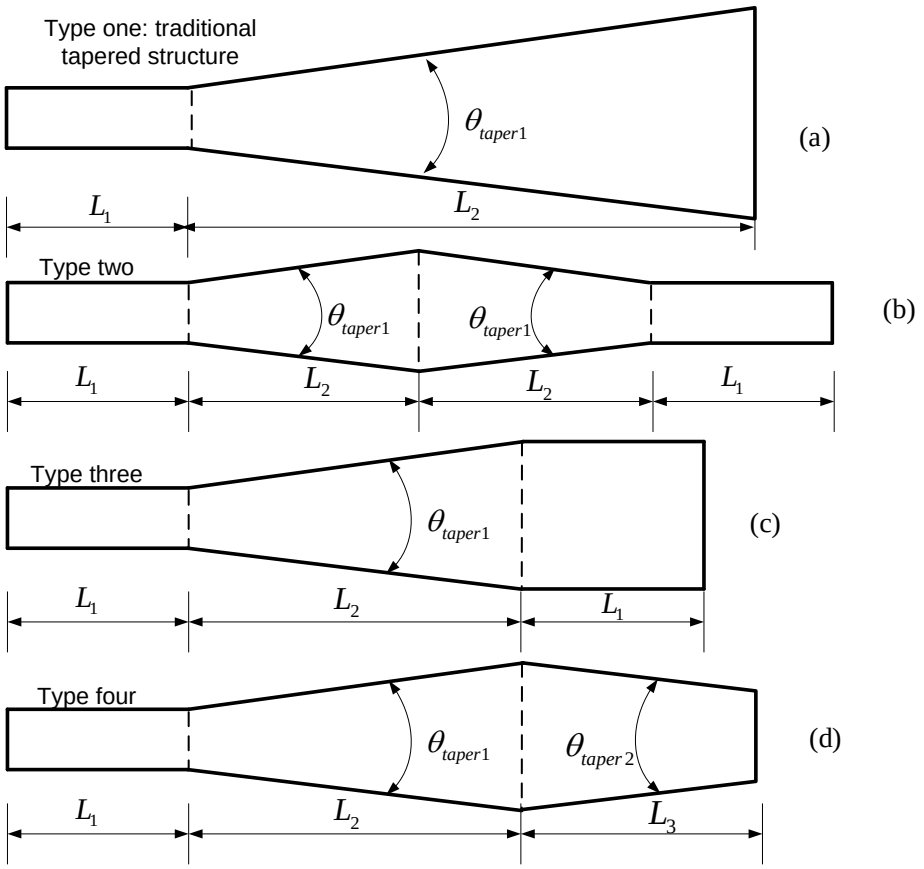


Fig. 3 Schematics of the considered four kinds of tapered waveguide.

The schematics of these four waveguide structures are shown in figure 3, and the related parameters are reported in table 1. Type one is the traditional type, which consists of a straight section and a tapered section. This kind of waveguide was experimentally proved to be efficient in multi-lateral mode prevention when the taper angle is smaller than 5 degree. While if increasing the taper angle to 8 degree, the output beam quality highly degrades at high injection current, which leads to lower usable output power as well, due to the poor coupling efficiency of the output beam [12, 18]. In order to overcome this problem, three different tapered waveguide structures are considered. All of them have the same total area to eliminate its impact on the output power. The middle parts of them all use taper sections with 8 degree angle. The only difference between them is the output section, which is designed aiming to improve the output beam quality at high injection current.

Tab. 1 Configuration parameters for the considered four THz QCLs.

| | $\theta_{taper1}/degree$ | $\theta_{taper2}/degree$ | $L_1/\mu m$ | $L_2/\mu m$ | $L_3/\mu m$ |
|---|---|---|---|---|---|
| Type one | 8 | / | 500 | 2500 | / |
| Type two | 8 | / | 500 | 1372 | / |
| Type three | 8 | / | 500 | 1820 | / |
| Type four | 8 | 5 | 500 | 1820 | 540 |

Optical intensity maps in the x-z plane for these four devices when $J = 430\ A/cm^2$ are shown in figure 4. We can see that the optical field is well confined within the waveguide because of the index guiding effect. Special attention should be paid to figure 4a, where we can see that after entering the taper section, the optical beam is broadened a little at the beginning part due to the increase in the waveguide width, but there is not obvious spread in the optical beam in the following part of this waveguide. Reason for this phenomenon is the so-called self-focusing effect which could be observed in the region with high optical intensity [20]. In addition, we found that under this current density all four devices have single lateral mode output beam profile.

Changes in the output power and the full width half maximum (FWHM) of the far-field laser beam versus the injection current are shown in figure 5. For the traditional tapered THz QCL (type one), the output power increase continuously with the injection current density, but there is a rapid increase in the far field FWHM angle at high injection current density. In order to get more insight on this phenomenon, the angular distributions of the normalized intensity of the far-field laser beam for device one are shown in figure 6a under different current densities. We can see that when $J = 430\ A/cm^2$ the output beam has well formed single lateral mode. While when $J = 522\ A/cm^2$ the output beam changes to multi-lateral mode, so the far field FWHM

increases rapidly. If we increase the current density continuously, the output beam still has multi-lateral mode, but far field FWHM decreases. Indeed, the output coupling efficiency of the laser beam depends directly on the output beam quality, therefore, this parameter for device one drops rapidly at high injection current. Consequently, the real output power that can be detected or utilized is considerably reduced at high current region. And this is the reason that the experimentally measured output power for device with 8 degree taper is lower than that for the device with 5 degree taper [12].

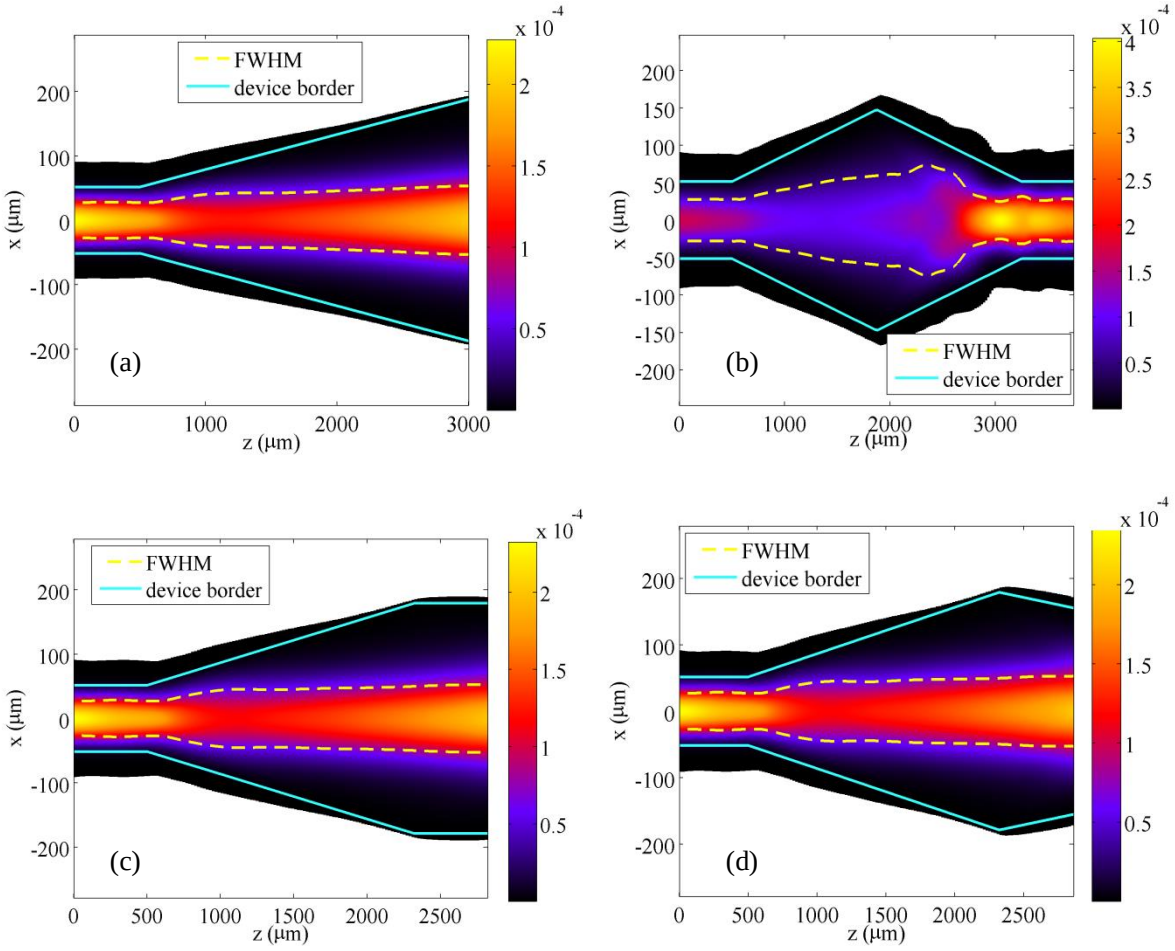


Fig. 4 Optical intensity maps in the *x-z* plane for the considered tapered THz QCLs when injection current density equals to 430 $A/cm^2$, with the solid lines indicating device active region and the dashed lines indicating the full-width at half maximum contour of the optical intensity.

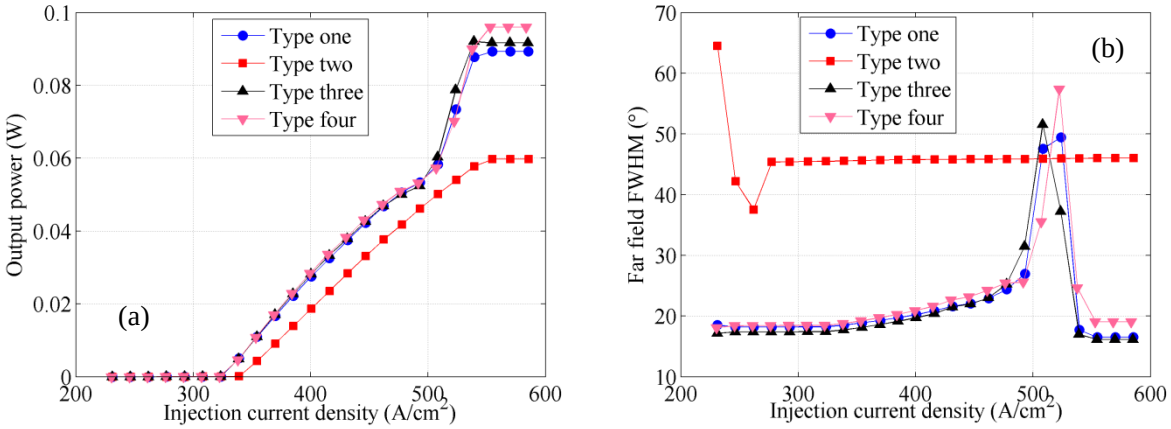


Fig. 5 Simulation results for the considered tapered THz QCLs: (a) the output power and (b) the far field full width half maximum as a function of the injection current density.

According to the simulation results in figure 5, we know that type two is the worst waveguide structure which has the lowest output power and largest far field FWHM angle due to narrow ridge at the output facet. In addition, it seems that there is no obvious improvement in the device performances when we change the waveguide structure to type three and type four. Multi-lateral mode output beam appears in the high current region also in these devices (see figure 6b).

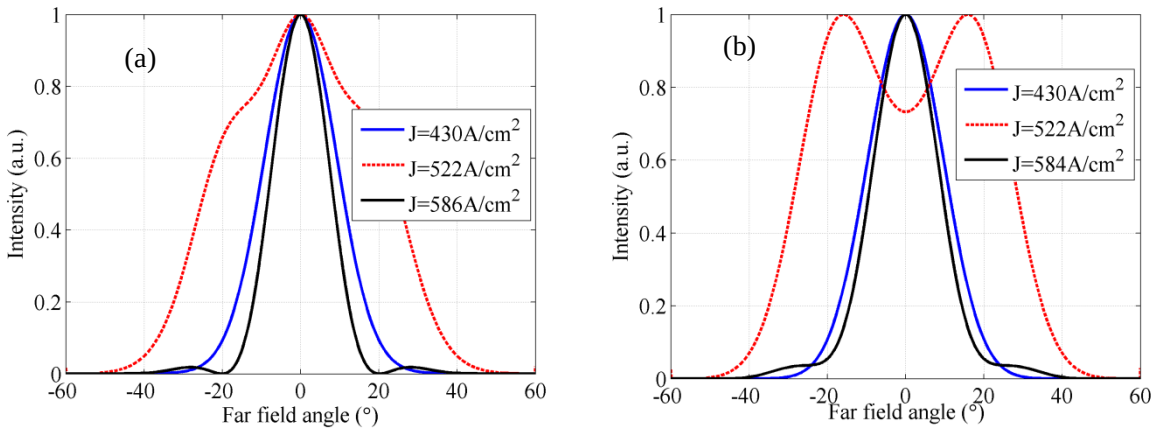


Fig. 6 Far field distributions when $J$ = 430 $A/cm^2$ (blue curve), 522 $A/cm^2$ (red curve) and 584 $A/cm^2$ (black curve), respectively, for the type one (a) and type four (b) THz QCLs.

Based on the analysis of four different tapered waveguide structures, we could get two main conclusions. First, the output power level relates tightly with the device area. We can see that the four THz QCLs used in this work have almost the same output power since they are designed to have the same area. Secondly, the output beam quality for 8 degree tapered THz QCL is not optimized by changing the waveguide structure of the final output section. It seems there is a strict upper limit for the taper angle if we want to get good output beam quality, i.e., when we design the THz QCL, we could choose the simple traditional tapered waveguide structure, but

there is an optimum value for the taper angle.

## 4. Conclusions

Four different tapered THz QCLs are investigated using the introduced FD-BPM model. We find that variations in the output section of the waveguide structure don't lead to obvious improvement in the device performances when comparing with the traditional tapered waveguide structure. And the key point to get high output power and good output beam quality simultaneously is to choose an optimum taper angle for the device.

## Acknowledgements

This work was supported by the 973 Program of China (Grant No. 2014CB339803), the National Natural Science Foundation of China (Grant Nos. 61131006，61321492), the Major National Development Project of Scientific Instrument and Equipment (Grant No. 2011YQ150021), the National Science and Technology Major Project (Grant No. 2011ZX02707), the International Collaboration and Innovation Program on High Mobility Materials Engineering of the Chinese Academy of Sciences, the Shanghai Municipal Commission of Science and Technology (Project No. 14530711300) , and the Shanghai Sailing Program (Project No. 15YF1414400).

## References

[1] J. Faist, F. Capasso, D. L. Sivco et al. "Quantum Cascade Laser". *Science*, 264, 553-556 (1994).

[2] R. Kohler, A. Tredicucci, F. Beltram et al. "Terahertz semiconductor-heterostructure laser". *Nature*, 417, 156-159 (2002).

[3] S. Kumar. "Recent Progress in Terahertz Quantum Cascade Lasers". *IEEE J. Select. Top. Quantum Electron.*, 17, 38-47 (2011).

[4] H. Li, Y. J. Han, Z. Y. Tan, et al. "Device fabrication of semi-insulating surface-plasmon terahertz quantum-cascade lasers". *Acta Phys. Sin.* 59, 2169-2172 (2010).

[5] W. J. Wan, R. Yin, Z. Y. Tan, et al. "Study of 2.9 THz quantum cascade laser based on bound-to-continuum transition". *Acta Phys. Sin.* 62, 210701-210705 (2013)

[6] B. S. Williams, S. Kumar, Q. Hu et al. "High-power terahertz quantum-cascade lasers". *Electron. Lett.*, 42, 89-91

(2006).

[7] B. Williams, S. Kumar, Q. Hu et al. "Operation of terahertz quantum-cascade lasers at 164 K in pulsed mode and at 117 K in continuous-wave mode". *Opt. Express,* 13, 3331-3339 (2005).

[8] L. Li, L. Chen, J. Zhu et al. "Terahertz quantum cascade lasers with >1 W output powers". *Electron. Lett.,* 50, 309-311 (2014).

[9] S. Kumar, Q. Hu, and J. L. Reno. "186 K operation of terahertz quantum-cascade lasers based on a diagonal design". *Appl. Phys. Lett.,* 94, 131105 (2009).

[10] S. Kumar, B. S. Williams, Q. Qin et al. "Surface-emitting distributed feedback terahertz quantum-cascade lasers in metal-metal waveguides". *Opt. Express,* 15, 113-128 (2007).

[11] D. Burghoff, T.-Y. Kao, N. Han et al. "Terahertz laser frequency combs". *Nat Photon,* 8, 462-467 (2014).

[12] Y. Li, J. Wang, N. Yang et al. "The output power and beam divergence behaviors of tapered terahertz quantum cascade lasers". *Opt. Express,* 21, 15998-16006 (2013).

[13] S. Kohen, B. S. Williams, and Q. Hu. "Electromagnetic modeling of terahertz quantum cascade laser waveguides and resonators". *J. Appl. Phys.,* 97, 053106-053109 (2005).

[14] K. Okamoto K. *Fundamentals of Optical Waveguides*, San Diego: Elsevier Inc., Chapter 1, 364-370 (2006).

[15] J.Q. Liu, J.Y. Chen, F.Q. Liu et al. "Terahertz Quantum Cascade Laser Operating at 2.94 THz". *Chin. Phys. Lett.,* 27, 104205 (2010).

[16] H. Li, J. M. Manceau, A. Andronico et al. "Coupled-cavity terahertz quantum cascade lasers for single mode operation". *Appl. Phys. Lett.,* 104, 241102 (2014).

[17] J. Wang, W. D. Wu, X. L. Zhang, et al. "Analysis of terahertz quantum cascade laser beam". *Chin. J. Comput. Phys.* 29, 127-132 (2012).

[18] T. H. Xu, C. Yao, W. J. Wan, et al. "Analysis of the output power and beam quality of the tapered terahertz quantum cascade lasers". *Acta Phys. Sin.,* accepted.

[19] L. A. Coldren and S. W. Corzine. *Diode Lasers and Photonic Integrated Circuits*, New York: John Wiley & Sons, Inc., Chapter 5, 209 (1995).

[20] J. R. Marciante and G. P. Agrawal. "Nonlinear mechanisms of filamentation in broad-area semiconductor lasers". *IEEE J. of Quantum Electron.,* 32, 590-596 (1996).